Part II

A charge transfer complex on a metallic surface: TTF-TCNQ on Au(111)

Introduction to charge-transfer complexes

Donor-acceptor interaction

Molecular charge-transfer complexes are based on the interaction between two molecular species, namely donor (D) and acceptor (A).

The donor molecule has a small ionization energy (IP), while the counterpart acceptor molecule has a large electronegativity or electron affinity (EA). When donor and acceptor interact, the charge is redistributed among the compound. The donor species oxidizes by the loss of charge and the acceptor is reduced. The result is a charge-transfer salt D_mA_n described by the following reaction [100]:

$$[D_m] + [A_n] \rightarrow [D_m]^{+\delta} + [A_n]^{-\delta}, \tag{4.3}$$

where δ is the charge-transfer ratio, and m and n are integers.

In some cases, these donor-acceptor interactions mediate the formation of charge-transfer crystalline solids in which organic molecules are stacked in homomolecular rows, being the molecular interactions within the chains of π-π character. The molecules pack rather densely in order to maximize the orbital overlapping between neighboring molecules and increase the charge transfer between the donor and acceptor counterparts.

This overlap facilitates the mobility of the charge carriers. Hence, the charge transferred among molecules will have a preferential delocalized π character. Therefore, the spatial arrangement of the molecular building blocks is important to determine the directions of charge motion.

The overlapping of π molecular orbitals leads to the formation of bands in the organic crystal, whose properties differ significantly from metallic bands. The density of free charge carriers is lower than in the case of a metal, and the effective carrier mass m* is typically larger than $1m_e$ [100].

A model case: TTF-TCNQ

Since its synthesis 35 years ago [101], the charge-transfer compound TTF-TCNQ has been considered a prototype of low-dimensional organic metal, exhibiting a room temperature conductivity of $400 \pm 100\ \Omega^{-1}cm^{1}$ [101, 102, 103]. It is formed by the com-

bination of donor (TTF, tetrathiafulvalene, $C_6H_4S_4$) and acceptor (TCNQ, 7,7,8,8-tetracyanoquinodimethane, $C_{12}H_4N_4$) molecules (Fig. 4.8(a)).

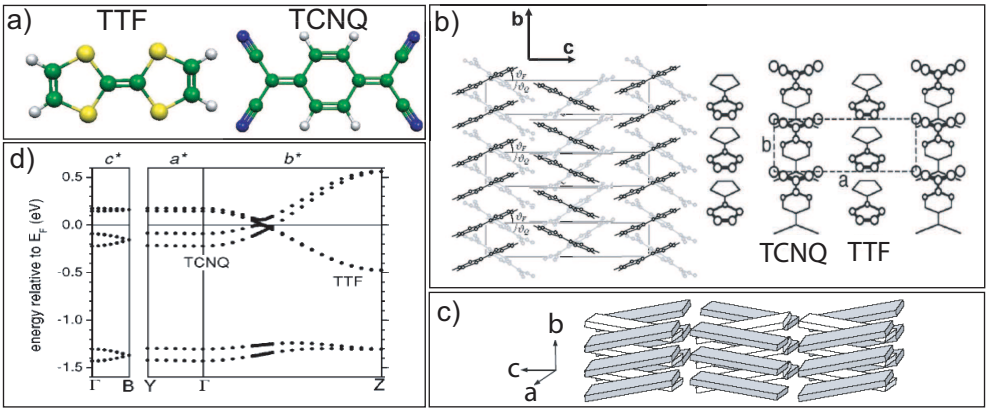

Figure 4.8: (a) Scheme of the TTF (left) and the TCNQ (right) molecules. Green spheres stand for C atoms, white for H atoms, yellow for S atoms, and blue for N. (b) Bulk structure of TTF-TCNQ showing the principle directions, a, b, and c, of the three-dimensional unit cell. Along a the charge transfer between cation and anion occurs, and it is delocalised along the direction of π-stacked rows, b [104, 105]. (c) Three-dimensional scheme of the TTF-TCNQ structure [106]. (d) Calculated band structure [105]. Dispersive behaviour is observed along the direction Γ-Z (b^*). The splitting of the bands indicate that molecular chains are not completely isolated from each other.

TTF has a strong donor character with a gas phase IP of 6.83 eV [107, 108]. This planar molecule is formed by two dithiolylidene rings, containing seven π electrons each (Fig. 4.8(a)). Its good donor properties are partly due to the gain in aromatization energy when it is oxidized. TTF can donate two electrons reversibly. Each donation results in a transformation of one of the dithiolylidene moieties in a dithiolium aromatic six π electron configuration [109, 110].

On the other hand TCNQ is a strong acceptor molecule. Its EA has been measured by means of collisional ionization technique [111], yielding a gas phase value of 2.8 ± 0.1 eV [112, 113]. TCNQ has two dicyanomethylene termination groups (C_3N_2) with strong electrophilic character [114]. The central part of TCNQ consists of a quinonoid ring that stabilizes the anionic system because it allows an efficient charge delocalization [115] (Fig. 4.8(a)). TCNQ exhibits in gas phase two successive one-electron reductions, both chemically and electrochemically reversible. This molecule can accommodate up to two electrons in the central ring that, upon charge injection, increases its aromaticity [116].

The formation of the organic crystal results from anisotropic non-covalent interactions between TTF and TCNQ. TTF-TCNQ crystallizes in a monoclinic structure built up from homologous stacks of TTF and TCNQ. The molecules overlap within the rows in a ´ring double bond´ fashion along direction b, as shown in Fig. 4.8(b) and (c) [117]. The direction a of the crystal corresponds to the alternating rows of TTF cations and TCNQ anions, stabilized by H-bonds [118]. The charge transferred

between the donor and acceptor molecules accounts to 0.59 e^- [119, 120].

The metallicity of the compound is due to (i) the formation of bands through the π overlapping of the molecular components, and (ii) the partial occupation of these bands at the Fermi level. The molecular packing maximizes the overlapping integral and, consequently, the amount of charge that can be delocalized along the stacks. The free carriers are generated in both π-stacked rows due to charge transfer between TTF and TCNQ. This transferred charge is delocalised along the b direction of the crystal resulting in a quasi one-dimensional electron dispersion as it has been both described by theoretical DFT calculations [105, 121, 122] (Fig. 4.8(d)) and observed experimentally [123].

As a quasi one-dimensional molecular metal, TTF-TCNQ undergoes structural transformation associated to Peierls instabilities. There is a transitional region between T = 54 K and T = 38 K dominated by one-dimensional distortions [124, 125] that develop charge density waves (CDW) on the ab surface of the crystal [104, 126]. Below 54 K TTF-TCNQ undergoes a sequence of phase transitions that progressively destroy the electronic transport [102], and affect the magnetic properties of the crystal [127, 128]

In contrast with an exhaustive study of the bulk properties, very little is known about the thin-film behavior, which have been studied only down to, approximately, 1 μm thickness on alkali halide substrates [129]. The transition from bulk TTF-TCNQ to thin films deposited on metals is expected to introduce new phenomenology related to the organic-inorganic interface. Effects like hybridization, charge transfer with the surface, and molecular level alignment become factors that may govern the electronic transport. Hence, the adsorption of ultra-thin TTF-TCNQ layers on a metal opens a new field of research, where the one-dimensionality exhibited by the bulk TTF-TCNQ and its related phenomenology may be exported to the metal-organic interface.

To have a better insight into the role played by each counterpart of the charge transfer complex and the properties emerging upon interaction with the Au(111) surface, we have studied the adsorption properties of TTF and TCNQ individually, prior to the combined co-deposition of both molecules. In the following chapters phenomena related to the TTF/Au(111), TCNQ/Au(111), and TTF-TCNQ/Au(111) interfaces will be discussed.

Chapter 5

Donor and acceptor molecules on Au(111)

This chapter is focused on the individual adsorption of TTF and TCNQ on Au(111). These molecules exhibit strong donor and acceptor properties when interacting in a charge transfer crystal. A naif approximation will assume that this character is unperturbed upon interaction with an electronic reservoir. But molecular adsorption on a metallic surface leads to, in a simplified picture, interaction of the molecular frontier orbitals (HOMO and LUMO) with the electrons of the surface. Depending on the energy level alignment and the degree of overlap with the metal Fermi level, the interactions may involve different charge transfer between molecules and surface [130], leading to changes on the electronic state of the molecules upon adsorption.

In the following sections we will characterize the electrical character of both molecules at the interface with a Au(111) surface. A combination of STS and DFT calculations will allow to understand the interaction of TTF and TCNQ with the underlying substrate and their charge state upon adsorption.

5.1 TTF on Au(111)

5.1.1 Long-range repulsive growth

The deposition of TTF at room temperature on Au(111) at four different coverages of 0.03 monolayers (ML), 0.04 ML, 0.08 ML, and 0.16 ML [1] leads to the formation of a quasi-periodic molecular superlattice (Fig. 5.1(a)-(d)). STM constant current images of TTF monomers are basically dominated by signal located at the S atoms and the ethylene bonds (Fig. 5.1(e)). Two of the S atoms appear brighter suggesting a small tilt of the molecular plane with respect to the surface (Fig. 5.1(f)).

Upon adsorption on a metal, it is expected for an apolar and neutral molecule like TTF to build self-assembled structures via short-range non-covalent attractive interactions [131]. In the present case, TTF molecules do not respond to such attractive interactions. Instead, they form spontaneously a monomer lattice as it is shown in

[1] The molecular coverage is determined from STM images of large surface areas, assuming that 1 ML corresponds to two molecules per nm^2.

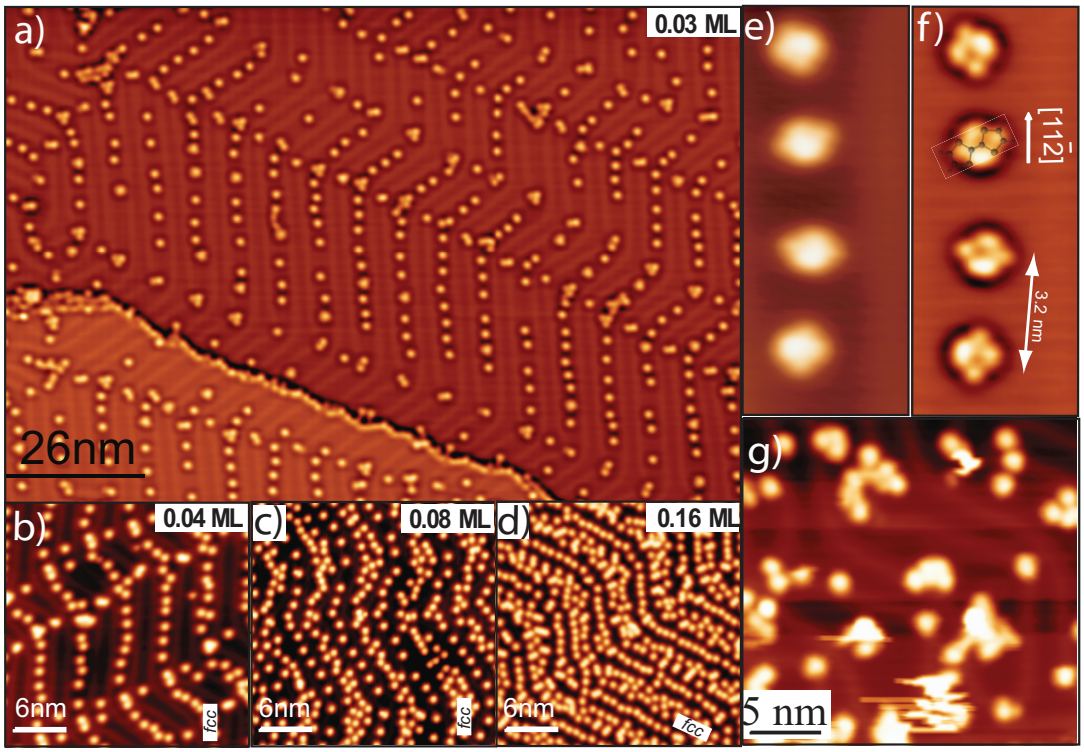

Figure 5.1: (a)-(d) STM images for different TTF coverages of 0.03 ML (V = 0.9 V, I = 0.3 nA) (a), 0.04 ML (V = 1.2 V, I = 0.2 nA) (b), 0.08 ML (V = 0.8 V, I = 0.1 nA) (c), and 0.16 ML (V = 1.2 V, I = 0.3 nA) (d). (e) STM image of four TTF monomers adsorbed on the fcc region of the reconstructed Au(111) surface (V = -1 V, I = 0.3 nA). (f) Laplace filtered image of (e). The STM signal is mainly located at the S atoms and the ethylene bonds as indicated by the TTF model superimposed to one TTF. The image reveals that two of the sulfur atoms for each molecule appear brighter suggesting a small tilt of the molecule plane with respect to the surface. (g) Deposition of molecules on a cold sample (80 K) leads to population of a weakly adsorbed precursor state, in which molecules may nucleate in clusters.

Fig.5.1(a)-(d). This behaviour prevails as the coverage is increased, being accompanied by a monotonous decrease in the average pair distance between the monomers.

For both 0.03 ML and 0.04 ML coverages, TTF only adsorbs in the fcc regions of the reconstructed Au(111) surface, forming one-dimensional chains of TTF monomers. Molecular adsorption at fcc sites might be favoured by the lower concentration of surface atoms compared to the hcp sites, where buried layers have to be taken into account [132]. At a coverage of 0.08 ML the array is compresed into a two-dimensional molecular distribution in the fcc region. Close to this coverage, the hcp region starts to be populated with similar one-dimensional arrays of TTF as observed in the fcc areas for lower coverages. Molecules are thus not compressed and self-assembled in the fcc area before they start to adsorb in the hcp regions of the Au(111) surface. This phenomenon can be considered as an indication of a repulsive interaction among the TTF molecules, since it is favourable for TTF to migrate to, in principle, more unfavorable regions of

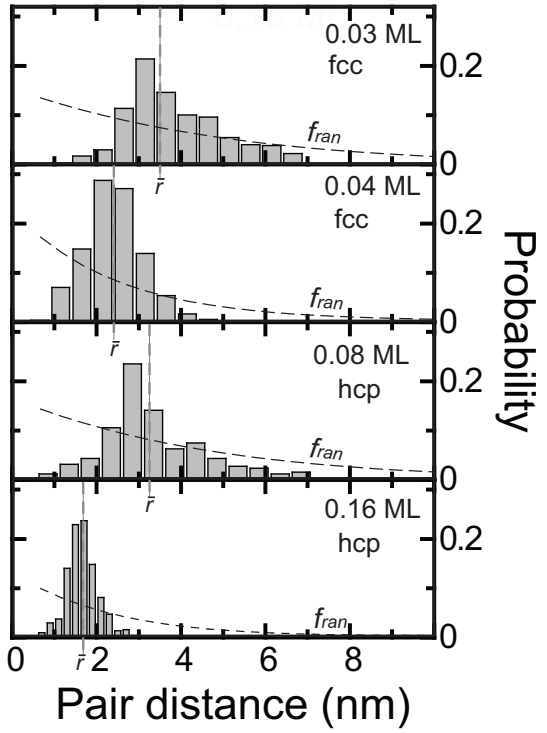

Figure 5.2: Pair distributions f of the one-dimensional TTF distributions for the data shown in Fig. 5.1 (a)-(d). For 0.08 ML and 0.16 ML the distributions are performed on hcp regions. The corresponding 1D random distribution function for non interacting particles, f_{ran}, is included.

the Au(111) surface in order to keep the TTF molecules separated.

The formation of this superlattice of TTF monomers needs to be thermally activated. Molecular deposition at a surface temperature of 80 K results in a disordered arrangement of TTF molecules (Fig. 5.1(g)) where molecules are randomly spread in the fcc and hcp regions of the Au(111) surface, and are easily dragged by the STM tip due to the weak adsorption on the surface. Only upon annealing (at room temperature) the molecules self-organize and form the periodic arrays. Further annealing at temperatures of, typically, 340 K, does not yield to island formation. Hence, we can assume the TTF superlattice is a stable configuration.

To get an insight on the origin of this monomer superlattice we perform a quantitative analysis of the one-dimensional average pair distance for the four different coverages investigated (Fig. 5.2). The statistics are taken over 500 molecular pairs per plot. In the cases of 0.03 ML and 0.04 ML coverages, the one-dimensional distribution statistics are carried out in the fcc domains, since hcp areas are not yet populated. On the other hand, for 0.08 ML and 0.16 ML, pair distances are measured only in hcp areas because of the two-dimensional distribution present in fcc sites at such coverages. The distributions are peaked with a dominant average pair distance, with values of 3.5 nm (fcc), 2.5 nm (fcc), 3.3 nm (hcp), and 1.7 nm (hcp), from the lowest to the highest coverage, respectively.

A comparison with a one-dimensional random distribution, f_{ran}, corresponding to non interacting particles for each coverage is plotted in Fig. 5.2. The one-dimensional random separation distribution is expressed, in analogy to two-dimensional distributions [133], as:

$$f_{ran} = \frac{Nar}{L}\left\{1 - \frac{2r}{L}\right\}^N \tag{5.1}$$

where N is the number of molecules per image, L is the length of the one-dimensional row, a is the minimum size of the box which can fit a molecule inside, and r is the intermolecular pair distance. For this system of non-interacting particles, the nearest neighbors random pair distribution decays monotonously with the pair distance r. Therefore, the experimental peaked distributions obtained can not be explained by a random adsorption of monomers, but are symptomatic of a repulsive interaction.

The random distribution f_{ran} and the experimental statistics reach an agreement in the case of long pair distances, above $\sim$ 4-5 nm (tail of both experimental and random distributions) and low coverages (see for example the coverages corresponding to 0.03 ML and 0.08 ML in fcc and hcp regions, respectively). For the limit of a very dilute system (low coverage), the interaction between the molecules located at large distances is almost negligible and the long intermolecular separations can be observed as a consequence of a random distribution. As long as the density of TTF monomers increases, the random factor loses importance and the distribution is ruled by a repulsive interaction. The formation of the superlattice is thus reinforced with the density of TTF monomers.

There are several mechanisms that can explain the origin of this long-range repulsive interaction among neutral molecules. Elastic deformations of the underlying surface created by dislocations [134] or vacancy islands [135] could lead to long-range interactions between adsorbates. For example, a chemical interaction between adsorbate and surface through strong S-Au bonds could reorganize the charge at the interface leading to an increase in the tensile surface stress [136]. In our case, the reconstructed Au(111) surface is already a stressed layer very sensitive to small distortions. For tensile stress to be the reason of the generation of the molecular superlattice, it is expected that some irregularities on the herringbone Au(111) reconstruction appear. Since this effect is not observed for any of the coverages studied, this explanation can be ruled out as the reason of the long-range interaction.

Friedel oscillations of the two-dimensional electronic gas associated with the surface state induce long-range adsorbate interactions [133, 137, 138, 139, 140, 141, 142, 143]. A key element in this case is the oscillatory character of the interactions associated to half the Fermi wavelength (λ_F), which amounts to a value of 1.8 nm for the Au(111) surface [138]. The STM images presented in Fig. 5.1 show a larger average pair distance than $\lambda_F/2$ and a monotonously decrease for larger concentrations of TTF molecules along the rows. Therefore, an interaction mediated by surface electrons can also be discarded as the force responsible for the superlattice formation.

A third mechanism is related to a possible dipolar nature of the adsorbates. The adsorption of molecules with an intrinsic dipole on a metallic surface creates a redistribution of charge at the organic-metal interface that reinforces the strength of the electrostatic interaction [144]. Even though TTF is considered to be apolar, its strong donor character can create a charge redistribution at the TTF/Au(111) interface, re-

sponsible for a repulsive interaction of electrostatic nature.

In order to confirm this hypothesis we have performed ab-initio calculations of the metal-organic system. These calculations provide information about the local molecule-surface interaction and its effect in a long-range repulsive molecular network.

5.1.2 DFT modeling of the TTF/Au(111) interface

Theoretical calculations have been carried out by Sergio Monturet and Prof. Nicolás Lorente[2], at the University of Paul Sabatier, Toulouse (France). According to DFT modelling, the interaction of the molecule with the surface is driven by local S–Au bonds. Due to the incommensurate dimensions of molecule and surface, the local interactions lead to a tilted chemisorption of the molecule. Two sulfur atoms are located on top Au sites forming a covalent S–Au bond, while the other two sulfur atoms are adsorbed on bridge and hollow sites (Fig. 5.3(a)). As a result, the molecule aligns along the $[1\bar{1}0]$ direction of the surface and tilts 8° with respect to the surface plane. The tilt is responsible for the asymmetry in the experimental constant current STM image (Fig. 5.1(f)) and it is also reflected by its Tersoff-Hamann simulation [16] (Fig. 5.3(b)). At negative bias voltage, the STM image is basically dominated by the shape of the HOMO with signal related to the DOS located mainly at the S atoms and ethylene bonds.

The local character of the interaction between Au and S atoms implies a large charge donation into the surface. The adsorption energy after dipole corrections is -0.86 eV, and the surface-molecule distance is 2.76 Å (S–Au bond distance). The electronic structure of the S atoms has a large contribution in the highest occupied molecular orbital (HOMO), what causes a large redistribution of electronic charge (Fig. 5.3(c)). The result is a positive charging of the molecule and the creation of a surplus of negative charge localized close to the S–Au bonds, as shown in the induced electronic density plot (Fig. 5.3(c)) and completed by the planar integration of charge (Fig. 5.3(d)). An excess of positive charge ($\sim 0.6\, e^-$) is located above the molecule and the corresponding screening negative charge ($\sim -0.4\, e^-$) is between the molecule and the first atomic layer. The molecule-surface interaction leads to a large surface dipole that is evaluated in Fig. 5.3(e) according to Ref. [145]. The dipole is zero inside the surface and builds up across the molecule reaching a value of 5.0 D.

The charge donation from TTF into the surface causes the partial emptying of the HOMO. This is clearly seen by plotting the projection of the full electronic structure onto the molecular orbitals corresponding to the present molecular conformation (Fig. 5.3(f)) [146].

The molecule-surface interaction also broadens the molecular features associated to the HOMO-1, HOMO and the lowest unoccupied molecular orbital (LUMO), revealing a substantial hybridization with the surface electronic structure, while higher-lying resonances are thinner reflecting their small role in the molecular-surface interaction.

[2]now at CIN2-CSIC, Barcelona

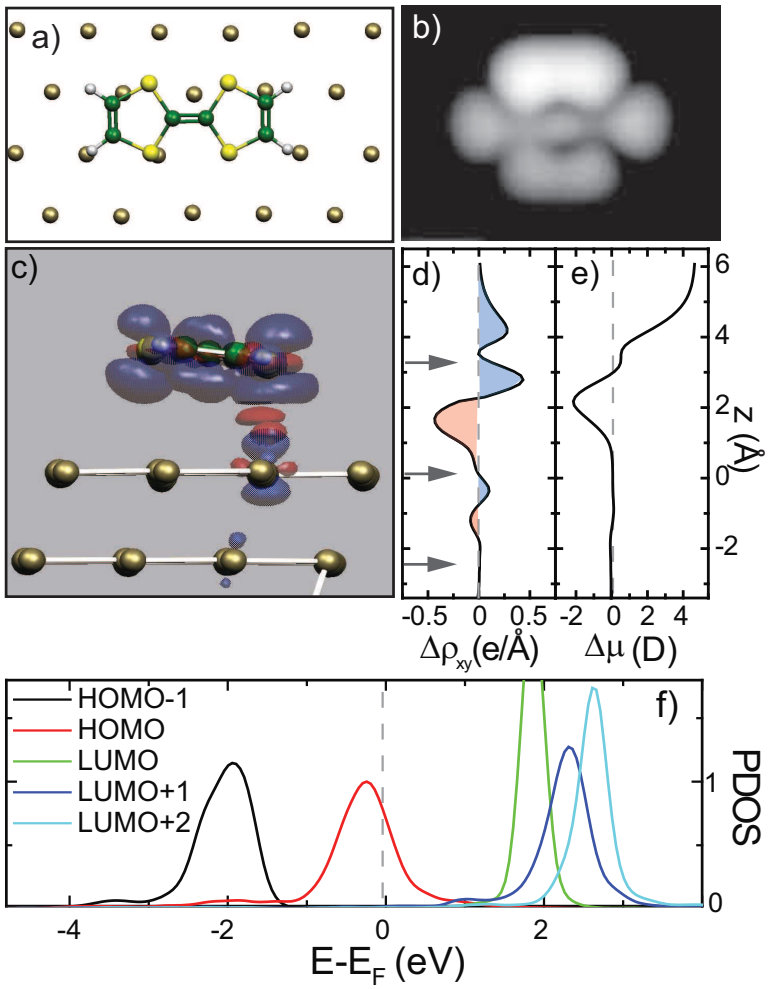

Figure 5.3: Results from DFT simulations. (a) Fully relaxed configuration of TTF on Au(111). The uppermost two gold layers as well as the molecular degrees of freedom are relaxed until atomic forces are lower than 0.01 eV/Å. (b) Tersoff-Hamann constant current image [16] of the molecule in (a) (V=-0.5 V). LDOS signal is mainly located on S atoms and on ethylene bonds. (c) Induced electronic density by the molecule–surface interaction. (d) Lateral (x-y planes) integration of the induced charge. The arrows show the vertical distance values at which the two topmost surface layers and the two binding S atoms lie. (e) Accumulated induced dipole. Together with (d) it reveals that the molecule becomes positively charged. (f) Projected density of states on molecular orbitals. The electronic states with HOMO character are partially empty, in agreement with the data of (c-e).

5.1.3 Formation of a molecular superlattice

The ab-initio results evidence a significative charging of the TTF upon adsorption on the Au(111) surface. To clarify its role in the formation of the arrays we analyze the statistics shown in Fig. 5.2. If we assume the system to be classical (distinguishable particles in a one-dimensional box) and in thermal equilibrium, experimental f_{exp} and

random f_{ran} distributions are related to each other by a Boltzmann factor [147].

$$f_{exp} = f_{ran} exp\left\{\frac{-(\omega(r) - \mu)}{k_B T}\right\} \tag{5.2}$$

where T is the temperature of the system and k_B the Boltzmann´s constant. $\omega(r)$ is the mean interaction potential that yields the formation of the superlattice, i.e., the monomer binding energy. It has a dependence on the intermolecular pair distance r. μ is an internal potential, representing the internal energy per molecule of a dense system of interacting particles. It is approximated by the electrostatic energy per molecule in a fully periodic one-dimensional lattice. In the case of an infinite number of particles this quantity μ can be associated to the thermodynamic chemical potential. This potential is defined, on a canonical collective described in terms of temperature, volume and number of particles, as the amount by which the energy of the system would change by the introduction (or removal) of a particle in the ensemble [148]. For the hypothetical case of infinite number of particles in a one-dimensional line the electrostatic interaction would be homogeneous among the uniformly distributed particles because there is no border effect. In that case the system is in equilibrium and it is possible to talk about a chemical potential.

From Eq. 5.2 the following result can be deduced:

$$\frac{\omega(r)}{k_B T} = \frac{\mu}{k_B T} - \ln\left\{\frac{f_{exp}}{f_{ran}}\right\} \tag{5.3}$$

Eq. 5.3 allows us to evaluate the factor $\omega(r)/k_B T$ as the combination of a zeroth order potential, $\mu/k_B T$, and a linear factor dependent on r, $\ln(f_{exp}/f_{ran})$. The results are presented, for the four different coverages, in Fig. 5.4.

In the limit of a very dilute system $\omega(r)$ is expected to be a good approximation for the repulsive pair interaction potential and to decay as $1/r^n$ [3] with the intermolecular distance [144]. Instead, $\omega(r)$ has the shape of a potential well for all the coverages, being more symmetric and shallower for larger TTF densities. This shape confirms the idea of the formation of a superlattice, in agreement with the TTF molecules being confined in sharper pair distributions for larger coverages.

For small pair distances, $\omega(r)$ decays as $1/r$ for all the coverages and is consistent with an electrostatic repulsion between charged molecules. In order to fit the $1/r$ behaviour of the mean potential for pair distances smaller than 3 nm, it is necessary to introduce a "vertical offset" related to the coverage-dependent zeroth order potential $\mu/k_B T$. This factor is calculated from the coulombic potential energy that the charges located in the one-dimensional system generate on each other:

$$\mu_{ij} = \frac{1}{4\pi\varepsilon_0}\frac{q_i qj}{r} \tag{5.4}$$

where $q_i = q_j = 0.3\ e^-$, corresponding to the charge obtained from the *ab initio* calculations, and r is the average pair distance for each of the studied coverages. As a

[3] The value of n depends on the nature of the repulsive interaction: n = 1 for a Coulomb repulsion, and n = 3 for a dipole-dipole interaction between the TTF monomers

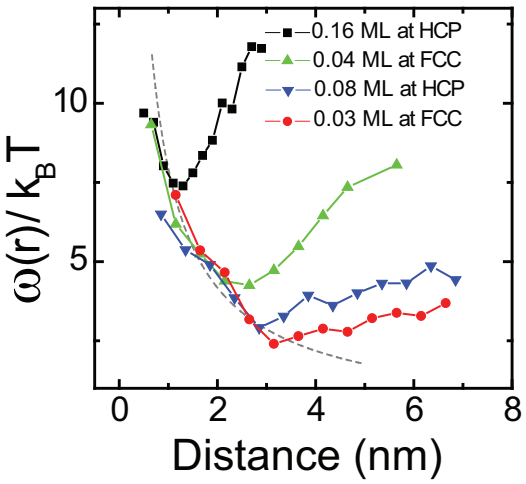

Figure 5.4: Mean interaction potentials $\omega(r)$ of one-dimensional TTF arrays obtained from the pair distributions shown in Fig. 5.2(d). The dashed line represents the pair electrostatic interaction E(r) between particles charged with 0.3 e^- and a temperature (T=165 K) to fit the repulsive part of $\omega(r)$ for the most dilute case. Each curve has been shifted upwards an amount (8.4, 5.4, 4.1, 3.8, from top to bottom) representing the coverage dependent zeroth order internal potential, approximated here as the electrostatic energy per molecule in a fully periodic lattice. The range of the interaction energy obtained from this fitting (55-114 meV) is considerably larger than the energy of a long range interaction mediated by surface electrons [139].

result we obtain values of interaction, for the first two neighbors[4], in a range between 55 meV and 114 meV, from the lowest to the largest coverages, respectively. The conversion of these offset interaction potentials in units of k_BT requires the fitting of a temperature. The average temperature necessary to match the decay at small distances of the four curves to a repulsive $1/r$ behaviour is 165 K (obtained from the average of values ranging from 158 K to 170K).

This temperature can be associated to the threshold required to start the formation of the monomer superlattice. Hence, for surface temperatures below $\sim$ 165 K, TTF would adsorb in a precursor state of disordered molecular clusters as presented in Fig. 5.1(g). Only when the temperature of the surface rises above 165 K the molecules are allowed to diffuse and order following a repulsive long-range interaction of coulombic nature.

The interaction mechanism suggested from the dependence of $\omega(r)/k_BT$ on the pair distance and the coverage is schematized in Fig. 5.5. For low TTF densities on the metal surface, the repulsive interaction is purely coulombic (Fig. 5.5(a)), while the aggregation of more charged molecules activates the creation of the superlattice, with shallower potentials located at the TTF monomers (Fig. 5.5(b)). This system can be compared, thus, to a one-dimensional molecular Wigner crystal created by charge transfer localized at the metal-organic interface [149].

[4]The neighbours considered are located at distances r and $2r$.

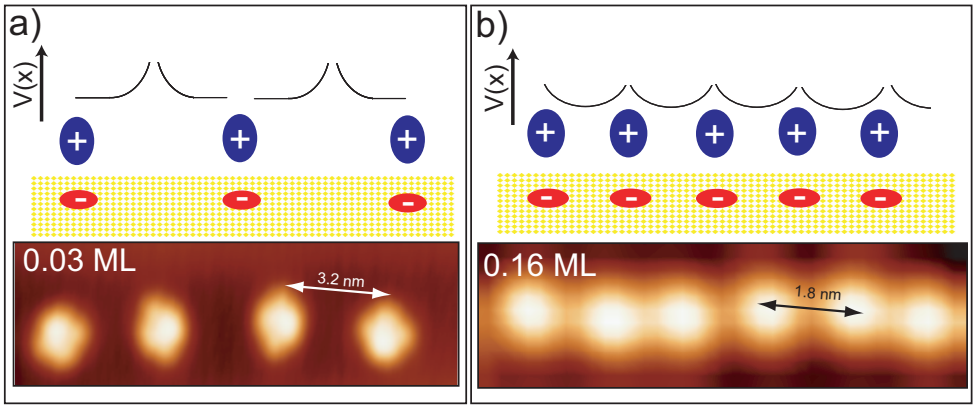

Figure 5.5: Scheme of the interaction potential dependent on adsorbates density. (a) sketches the case of a dilute system where the decay of the repulsive interaction is in a good approximation to $1/r$. (b) presents the formation of the electrostatic lattice for larger molecular coverages.

5.1.4 TTF nucleation: Long-range repulsive versus short-range attractive interactions

While the adsorption of small coverages (less than 0.16 ML) leads to the formation of a superlattice characterized by the repulsive interaction between charged molecules, further deposition of TTF on Au(111) results in molecular organization in self-assembled structures.

Upon deposition of $\sim$ 0.5 ML, TTF forms zig-zag chain-like structures uniformly distributed over the surface (5.6(a) and (b)). These chains exhibit a labyrinthine pattern that varies on the hcp and fcc sites of the reconstructed Au(111) surface. While in the fcc domains the chains tend to have a short length and several orientations, in the hcp regions the tendency is reversed with a preferential formation of long chains along the soliton lines. STM images with intra-molecular resolution resolves the relative orientation of the TTF molecules within the zig-zag chains (Fig. 5.6(b)). TTF molecules adsorb slightly shifted within the chains, being the structure dominated by S$\cdots$HC hydrogen bonds [150].

A larger coverage of $\sim$ 0.8 ML induces the formation of two-dimensional TTF islands (Fig. 5.6 (c) and (d)). Here, molecules pack densely in a parquet-like structure where adjacent molecules are rotated 60° to form a saturated S$\cdots$HC network. The areas covered by one-dimensional TTF chains exhibit the same zig-zag structure previously observed in the 0.5 ML coverage.

The characteristic laberynthine pattern obtained for large TTF densities is a fingerprint of a system grown with competing long-range repulsive and short-range attractive interactions [151, 152]. The strength of the competing interactions varies with TTF density. In the low coverage region, below $\sim$ 0.2 ML, the repulsive interaction is dominant and is the driving force responsible for the monomer superlattice formation. For medium coverages, ranging between $\sim$ 0.2 - 0.8 ML, both repulsive and attractive interactions play a role in the TTF self-organization resulting in a delicate balance.

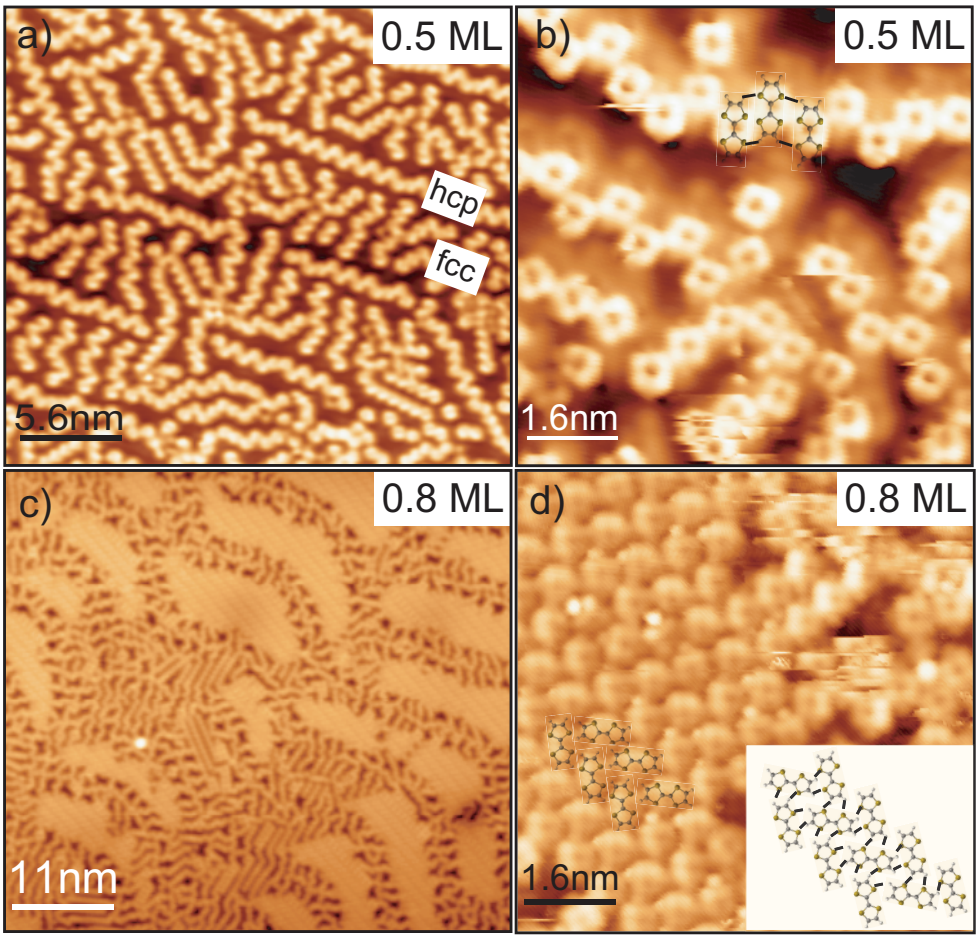

Figure 5.6: (a) Large STM image corresponding to a 0.5 ML TTF coverage (V = -0.05 V, I = 0.2 nA). The molecules adsorb forming labyrinthine patterns dependent on the reconstructed Au(111) surface. (b) STM zoom in a small domain with sub-molecular resolution (V = -0.03 V, I = 0.34 nA). The STM signal at the ethylene bonds allows to model the self-assembled structure via S–HC bonds. (c) Large image corresponding to a 0.8 ML TTF coverage (V = 0.7 V, I = 0.13 nA). The molecules self-assemble in two-dimensional islands with a packed herringbone structure (d) (V = -0.04 V, I = 2.2 nA). The inset shows a proposal for the saturated S$\cdots$HC network that forms the islands.

Above $\sim$ 0.8 ML island formation is predominant, as a consequence of the dominant short-range attractive interaction.

5.2 TCNQ on Au(111): A physisorbed acceptor layer

TCNQ is the acceptor counterpart of TTF in the TTF-TCNQ charge transfer salt. At positive sample bias voltages, STM images this molecule as two symmetric U-shapes with a nodal plane located at the middle of the quinonoid ring. An additional protrusion is found at the center of the dicyanomethylene groups (Fig 5.7(b)). This shape strongly resembles the isosurface of LUMO resonance of the free molecule (Fig 5.7(a)), as determined by semiempirical calculations. For negative bias voltages, TCNQ is imaged as a bright protrusion, without any internal molecular resolution (Fig 5.7(d)).

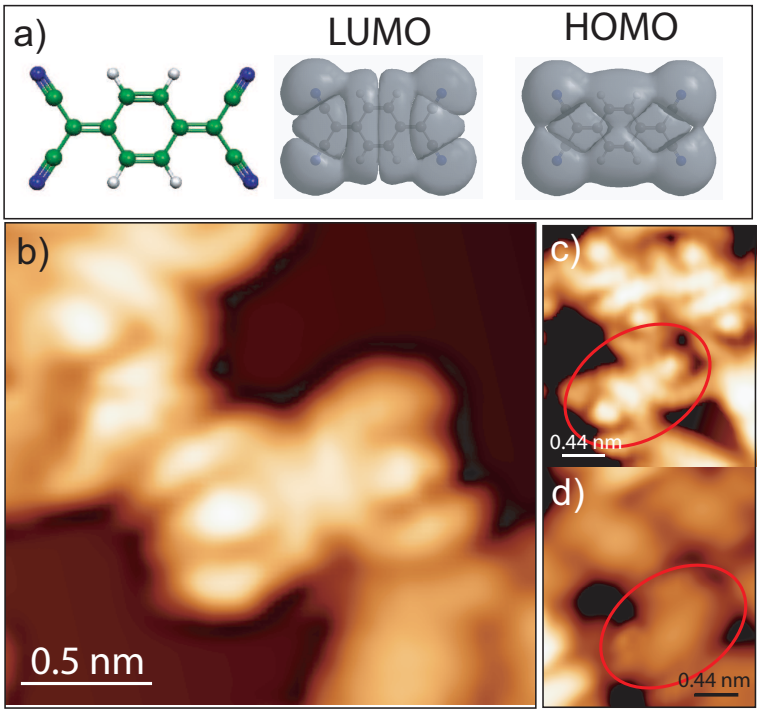

Figure 5.7: (a) Molecular model of TCNQ. Green circles represent C atoms, blue are N, and white are H. The grey surfaces are the isosurfaces corresponding to LUMO and HOMO obtained after relaxation of the free molecule. (b) TCNQ molecule imaged at positive bias voltage (V = 0.8 V, I = 0.32 nA). The LDOS resembles the LUMO shape of the free molecule, as can be observed by direct comparison with the isosurfaces presented in (a). (c) and (d) show STM images of the same TCNQ group taken at positive (c: V = 1 V, I = 0.33 nA) and negative (d: V = -1 V, I = 0.33 nA) bias voltages. At negative bias voltages TCNQ is imaged by STM as a homogeneous protrusion, without internal resolution.

Room temperature deposition of TCNQ onto a Au(111) surface results in the formation of highly ordered TCNQ self-assembled domains that extend over hundreds of Ånsgtroms onto the substrate (Fig. 5.8(a)). The STM images show, superim-

posed to the molecular corrugation, the unperturbed pattern of the herringbone reconstructed surface. This is a characteristic fingerprint of a weak adsorption on the surface. The strong resemblance of the molecular orbitals to the LUMO isosurface of the free molecule (Fig. 5.8(b)) corroborates the weak adsorption assumption. These results suggest that TCNQ, in contrast to the reported bent adsorption of its fluorinated derivative F_4-TCNQ on Cu(111) [153], has in this case a planar adsorption parallel to the metal.

Despite this physisorbed state, TCNQ exhibits a certain degree of commensuration with the Au(111) lattice. The molecular structure formed has a rhombic unit cell with vectors $a_1 \sim a_2 \sim 1$ nm (Fig. 5.8(b)). A simple model that accounts for both this lattice parameters and a commensuration with the underlying gold lattice is depicted in Fig. 5.8(c). According to this model, TCNQ molecules align in rows rotated almost 90°. The vector a_1 runs along the family of $\{11\bar{2}\}$ surface directions and a_2 presents a slight deviation of $\sim 5°$ with respect to the perpendicular direction. As a result, TCNQ molecules alternate two adsorption sites, one with the C atoms of the central ring on Au(111) hollow sites and other where C atoms are distributed on bridge and top sites.

The self-assembled structure is stabilized via a saturated C≡N$\cdots$H-C hydrogen bond network (Fig. 5.8(c)). All N and H terminal atoms are directly involved in the formation of bonds. The interatomic distance amounts to ~ 3 Å. This length is slightly larger than the interatomic hydrogen bond distances reported in liquid and gas phase complexes [154]. Therefore, even though TCNQ exhibits a weak adsorption on the metal surface, the formation of the C≡N$\cdots$H-C hydrogen bond network maintains a commensuration with the surface.

The weak interaction with the surface and the tendency to form a self-assembled network is in contrast to the results previously reported at the TTF/Au(111) interface. The formation of such ordered structure is not in agreement with a tendency of the molecule to accept charge from the substrate. Despite the strong acceptor character of TCNQ, there is no sign of charge transfer between the molecule and the surface. We expect that either TCNQ is essentially neutral on the Au(111) surface, or the attractive nature of C≡N$\cdots$H-C bonds destroys the effect of electrostatic repulsion between the negatively charged molecules. In order to solve these questions we have performed STS measurements at the TCNQ/Au(111) interface.

The conductance spectra exhibit two fingerprints non-existent on the bare Au(111) surface (Fig. 5.9(d)). The first is an unoccupied resonance located at 0.7 eV. The second is a shift of the Au(111) surface state of 150 meV towards the Fermi level. These two quantities are helpful to extract some information about the TCNQ/Au(111) interface as it is developed next.

The molecular resonance can be identified by the analysis of topography images with intramolecular resolution taken at several bias voltages. Both at negative sample bias voltages (tunneling from occupied states of the metal + molecule system) and at low positive bias voltages TCNQ molecules are imaged as featureless protrusions (Fig. 5.9(a) and (b) respectively). However, the contours of the local density of states approach the shape of the LUMO free molecule isosurface for bias voltages close to 0.7 eV and above (Fig. 5.9(c)). For molecules weakly adsorbed on surfaces, the intramolecular structure resolved by STM can be usually correlated to the shape of the molecular

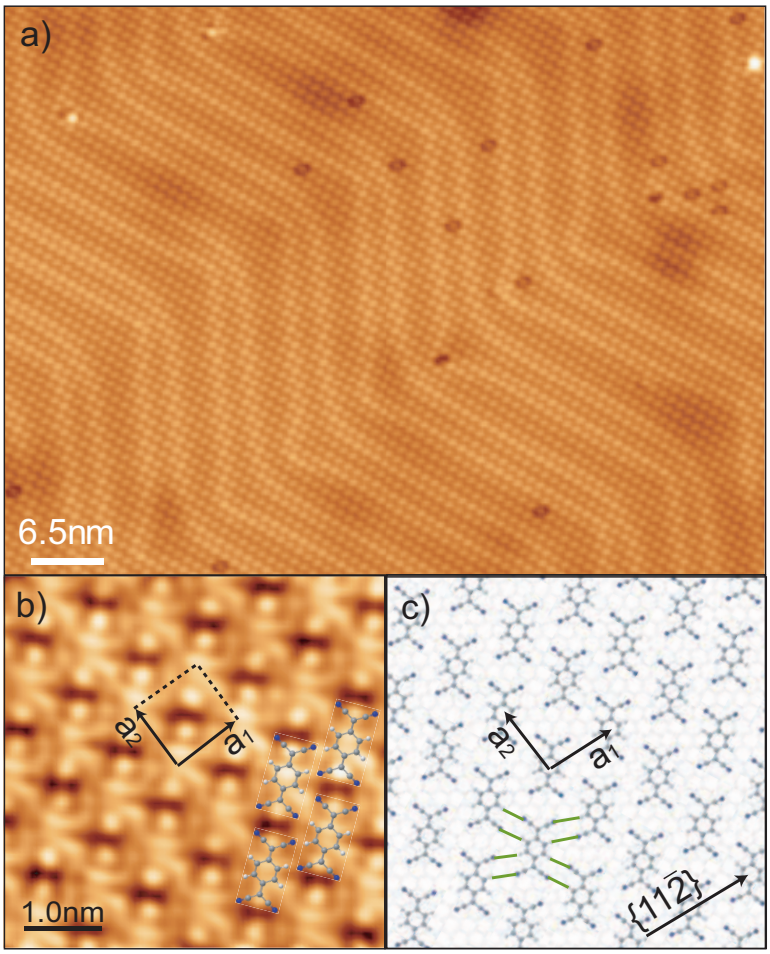

Figure 5.8: (a) Large STM area of a self-assembled domain of TCNQ. The reconstructed Au(111) surface with the characteristic herringbone pattern is visible through the molecular island. (b) Zoom with intramolecular resolution in a TCNQ island. The unit cell of the self-organized TCNQ domain exhibits a rhombic symmetry. The length of vectors a_1 and a_2 is $\sim$ 1 nm, and the angle between them is $\sim 90°$. Four TCNQ molecular models are superimposed on the molecular lattice to clarify the dimensions and orientation of the TCNQ monomers. (c) Adsorption model of TCNQ on Au(111). Molecules alternate two adsorption sites. Green lines mark the C$\equiv$N$\cdots$H-C bonds existing in one molecule. All the H and N terminal groups are involved in the attractive interaction.

orbitals [39]. Therefore, we can associate the STS peak at 0.7 eV with the LUMO derived resonance of TCNQ adsorbed on Au(111). The alignment of this unoccupied resonance far above the Fermi level suggests that there is no charge transfer involved in this state.

The second spectroscopic fingerprint involves a shift of the Au(111) surface state towards the Fermi level. Shifts of the metal surface state have been reported for

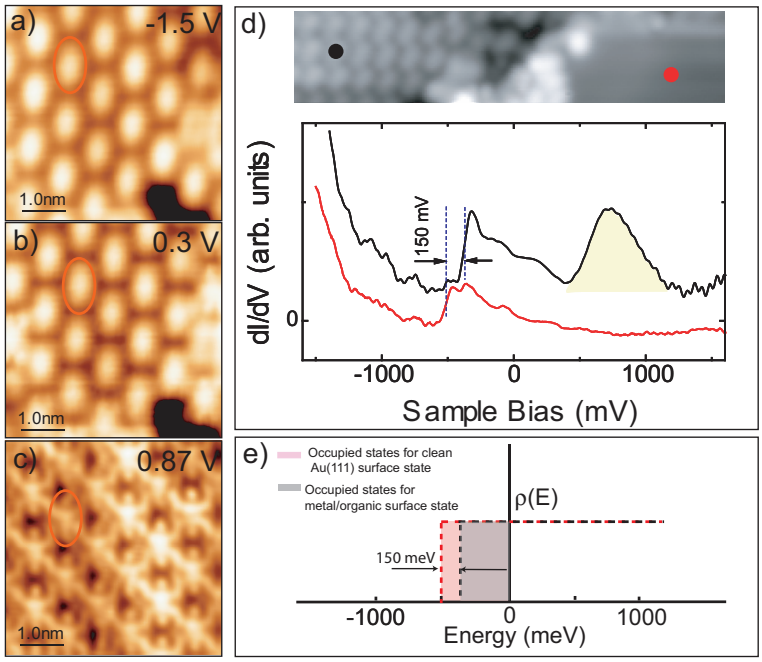

Figure 5.9: (a)-(c) Topography images of a self-aseembled TCNQ island, taken at different bias voltages. The intramolecular TCNQ LUMO-shape resolution is obtained for bias voltages close to 0.7 eV. (d) STS spectra taken on clean Au(111) (red curve) and TCNQ island (black curve). Parameters: V = 2V, I = 1.4 nA, V_{rms} = 7 mV. The black curve exhibits two features not observed on the spectrum of the metal, namely, a shift of the Au(111) surface state, and an unoccupied resonance at 0.7 eV.

different types of adsorbates on noble metal surfaces, like noble gases [155, 156, 157], insulating thin films [158], and molecular layers [159]. Its origin is attributed to either modifications of the image potential and/or surface work functions by the dielectric medium placed above the metal surface [158, 160, 161], or to surface state depopulation [162] produced by charge transfer processes at the molecule/metal interface.

Assuming that the upward shift of the surface state is due to electron depopulation, it is possible to estimate the amount of charge the surface would donate to the TCNQ molecule upon adsorption. The density of states of a two-dimensional system (in this case, the surface state) is a step function with an onset. For the clean Au(111) surface such onset is located at 490 meV below the Fermi level [31], as sketched in Fig. 5.9(e). The density of states is thus constant with a value of $m^*\pi/h^2$, where m* is the effective mass of the electrons in the Au(111) surface state, m*=0.28m_e [138, 163]. The amount of charge per unit of surface can be extracted from the integration of the area below the Fermi level. For clean Au(111) we obtain 0.0057 e^-Å^{-2}. For the covered surface the onset is shifted by 150 meV towards the Fermi level (Fig. 5.9(e)). If we assume the same dispersion for the electrons embedded at the organic/metal inteface, i.e., same value of the step function, the charge of the surface state is reduced to 0.0039 e^-Å^{-2}. Assuming an area of $\sim$ 140 Å^{-2} per TCNQ molecule, we obtain a transfer of charge

from the surface state towards the TCNQ of $0.2\ e^-$/TCNQ.

This value is comparable to the charge transfer previously reported for TTF on the same surface (0.3 e^-). However, in the TCNQ case we do not observe any charge transfer fingerprint in the molecular adsorbate structure. On the one hand, the molecules self-assemble in domains without any repulsive behavior due to a charge accumulation in the molecule. On the other hand this extra charge of 0.2 e^- should be also reflected in a lower energy alignment of the LUMO-derived resonance, partially crossing the Fermi level and becoming occupied. Our STS measurements establish the LUMO position at 0.7 eV (Fig. 5.9(d)), far away from E_F. Hence, we may tentatively assume that the shift of the Au(111) surface state is not due to charge transfer processes but produced by changes in the work-function and/or image potential shape induced by the molecular layer. In this case the shift should be accompanied by an increase in the electronic effective mass m*. Further measurements (STS or ARPES) are needed in order to provide a definite proof for this argument.

5.3 Conclusions

We have characterized the different adsorption properties of a charge donor (TTF) and an acceptor (TCNQ) on a Au(111) surface. Both molecules have potentially opposite electron transfer capabilities, but the different bonding to the surface imposes distinct behaviors upon adsorption.

In the case of TTF adsorbed on Au(111), the molecular chemisorption through covalent S–Au bonds results in a molecular scenario based in long range repulsive interactions of electrostatic nature that forms a molecular Wigner crystal. The charge that TTF donates to the surface upon adsorption leads to the creation of a molecular superlattice at low TTF coverages. The herringbone reconstruction of Au(111) with its fcc and hcp sites of different adsorption energy imposes a one-dimensional character to the molecular superlattice. DFT calculations helped to understand the nature of the bonding with the surface and explain the origin of the electrostatic lattice formation as due to a considerable charge transfer (0.3 e^- per molecule) towards the surface. For larger TTF coverages the repulsive interaction has to compete with a short-range hydrogen bonding force that comes into play due to the smaller distances between adsorbed molecules. Such competition depends strongly on the TTF density and leads to different self-assembled TTF patterns.

The growth of TCNQ on Au(111) follows a more familiar self-assembling process, common to many organic molecules deposited on surfaces. The weak bonding of the central aromatic ring and the ending CN groups with the surface prevent an appreciable charge transfer at the molecule/metal interface. TCNQ remains fairly unperturbed upon adsorption as proved by the free-molecule like orbital fingerprint observed at positive voltages. It is then expected for TCNQ to maintain the acceptor character in the adsorbed state. Even though TCNQ does not accept charge from the surface, it may become charged upon co-adsorption with molecules that exhibit strong donor character as is, for example, the case of TTF.